Synthesis of tin(IV) nitride with spinel structure, γ-Sn3N4, from the elements and its Raman-spectroscopic examination at high pressures

Andreas Zerr, Gerhard Miehe

Synthesis of tin(IV) nitride having spinel structure, γ-Sn_3N_4, from the elements and its Raman-spectroscopic examination at high-pressures

Andreas Zerr[1*] and Gerhard Miehe[2]

[1]*Laboratoire des Sciences des Procédés et des Matériaux, CNRS UPR 3407, Université Sorbonne Paris Nord, 99 av. J. B. Clement, 93430 Villetaneuse, France*

[2]*FB Material- und Geowissenschaften, Technische Universität Darmstadt, Alarich-Weiss-Straße 2, 64287 Darmstadt, Germany*

Keywords: spinel nitride, high pressure synthesis, Raman spectroscopy, powder X-ray diffraction, mode Grüneisen parameter, thermal shock resistance

We report on the synthesis of tin(IV) nitride having spinel structure, γ-Sn_3N_4, from the elements at high pressures and temperatures, using a laser-heated diamond anvil cell, and on the Rietveld refinement of the product structure. The described here procedure is, in our opinion, the most reliable method of obtaining high-purity nitrides which are thermodynamically only stable at high pressures. Raman spectroscopy and powder X-ray diffraction were used to characterise the synthesis products. Pressure dependences of the Raman-band frequencies of γ-Sn_3N_4 were measured and used to determine its average mode Grüneisen parameter $\langle\gamma\rangle$=0.95. Applying this value, we estimated thermal shock resistance of γ-Sn_3N_4 to be about half of that of γ-Si_3N_4 which, in turn, is moderately surpassed by β-Si_3N_4, known to be highly thermal-shock-resistant.

Introduction

Nitrides of the group 14 elements having spinel structure, γ-M_3N_4 (where M=Si, Ge, or Sn), and their solid solutions [1-5] are promising multifunctional materials which are not only hard and stiff e.g.[6-13] but were predicted to exhibit interesting optoelectronic properties answering actual demands in the energy consumption and functionality [14-16]. In particular, calculations based on the density functional theory (DFT) predicted direct band gaps for the end-members, γ-M_3N_4, as well as direct or nearly-direct band gaps for the solid solutions γ-$(Si_{1-x}Ge_x)_3N_4$ and γ-$(Ge_{1-x}Sn_x)_3N_4$ [12, 14, 15, 17]. Only recently, these predictions were confirmed experimentally for γ-Si_3N_4 and γ-Ge_3N_4 using the synchrotron-based photoluminescence (PL) and PL-excitation spectroscopy [18, 19]. Moreover, these experiments also confirmed the prediction of a large free-exciton binding energy, D_e, for γ-Si_3N_4 and γ-Ge_3N_4 [17] which is the second main prerequisite for an efficient conversion of electric power to light in light emitting diodes (LEDs). The presently used binary and ternary compounds of the group 13 and 15 elements (e.g. GaN, InN, (Ga,In)(N,As)) have much lower D_e [20]: For example, the D_e of GaAs (one of the most efficient LED materials in the IR-range of light) is only 4.2 meV while the earlier DFT calculations predicted for γ-Sn_3N_4, having a similar band gap of E_g =1.6(2) eV, D_e=69 meV [17]. The latter value combined with the thermal stability up to ~300°C [4, 10] suggests that an IR-LED based on γ-Sn_3N_4 should maintain a high energy-conversion efficiency at elevated electric currents passing through the *p-n* junction. Also, γ-Sn_3N_4 was shown to be one of very few materials combining a direct band gap of E_g<2 eV with alignment of its conduction and valence bands with the water redox potentials, needed for an efficient photo-electrochemical splitting of water [21]. The above properties and the possibility to deposit γ-Sn_3N_4 as thin films via economic magnetron sputtering [21-23] make γ-Sn_3N_4 an attractive candidate for the industrial production of green hydrogen. Finally, it is widely recognized that lattices of compounds having spinel structure possess an elevated neutron tolerance [24, 25] due to an efficient self-healing interstitial-vacancy (*i-v*) recombination process, the prerequisite of which is the presence of a huge number of so-called structural vacancies in the crystalline lattice. For compounds described by the general formula AB_2O_4, e.g. $MgAl_2O_4$, the energy costs of formation of antisites in the spinel structure are much lower than for all other elementary lattice defects [26]. This means that cation sub-lattice easily accommodates disorder or, in other words, is radiation tolerant. An even higher radiation

*Author for correspondence: Andreas Zerr (zerr@univ-paris13.fr).

tolerance is expected for single-cation spinels, such as γ-M_3N_4, because swapping of cation positions does not change anything in the lattice and, accordingly, results in null energy costs.

Despite a significant number of publications on the synthesis of tin nitrides in bulk [27-29] and as thin films [23, 30-33], an unambiguous evidence of the existence of stoichiometric Sn_3N_4 and its spinel structure was first reported in 1999 by Scotty et al. [4]. In this work, microcrystalline γ-Sn_3N_4 was obtained at atmospheric pressure via a reaction of a tin tetrahalide (SnI_4 or $SnBr_4$) with KNH_2 in liquid ammonia at -30 °C and subsequent decomposition of solid reaction products in vacuum at 300 °C. However, γ-Sn_3N_4 having good crystallinity was obtained only when elemental tin was present in the sample. Also, dissolving of the potassium halides, the second main reaction products, led to the appearance of tin oxides, SnO and SnO_2, in significant amounts, up to 23 wt.%. Attempts to purify the reaction products led to enormous losses of the material of interest [4]. For γ-Sn_3N_4, neutron as well as powder X-ray diffraction (XRD) data resulted in a cubic *F*-centred cell with the lattice parameter $a_0 = 9.037(3)$ Å and extinctions due to a *d*-glide plane, indications of a spinel-type structure (space group $Fd\,3m$, no. 227). In this structure, the cations occupy two different Wyckoff positions, 8*a* and 16*d*, and their coordinates (for the 2nd setting) are fixed at (1/8, 1/8, 1/8) and (1/2, 1/2, 1/2), respectively. The N-anions occupy the Wyckoff positions 32*e* with the coordinates, in the same setting, (*x*, *x*, *x*) which can be recovered from the structure refinement using the neutron- and/or XRD diffraction patterns. In their structure refinement, Scotty et al. obtained x=0.25950(6) (**Table 2**) and reported the R_{Bragg} value of 6.7% for γ-Sn_3N_4 [4].

The first high-pressure synthesis of γ-Sn_3N_4 was performed in a piston-cylinder apparatus by Shemkunas et al. [34] via a solid-state metathesis reaction of tin iodide (SnI_4) with lithium nitride (Li_3N) in the presence of ammonium chloride (NH_4Cl). The electron-probe microanalysis (EPMA) of the reaction product obtained at 2.5 GPa and 350 °C gave a nearly stoichiometric ratio of N:Sn=1.31 but also revealed about 1.8 at.% of oxygen and 1.05 at.% of chlorine in the sample. The powder XRD measurements on this product resulted in a smaller value for the lattice parameter, a_0=9.0144(1) Å, but positions of the N-anions were not determined. The size of crystallites in the annealed samples was considered to be larger than 10 nm. Furthermore, the authors reported a Raman spectrum of their γ-Sn_3N_4 at atmospheric pressure which showed four sharp peaks having frequencies of 160, 416, 524, and 622 cm^{-1} and a broad weak feature at ~252 cm^{-1}. Two more intense broad bands at ~470 and ~670 cm^{-1} were not attributed to γ-Sn_3N_4 [34]. Synthesis of γ-Sn_3N_4 from the elements in a laser heated diamond anvil cell (LH-DAC) was stated in two recent publications [35, 36] but the provided information was not substantial because no quantitative values but just illustrations in "Supporting information" were presented. Even though XRD patterns of the product were shown in "Supporting information" [35], neither the cubic lattice parameter was determined nor the structure refinement performed. Similarly, frequencies of the Raman bands at high pressures were shown in a Figure in "Supporting information" [36] but no numerical values provided. The reason for this scarce information was apparent: the two publications were devoted to the synthesis and characterisation of other Sn-N phases at pressures above the stability field of γ-Sn_3N_4. However, the illustrations and the measured specific volume of the product at high pressures reported in Refs. [35, 36] implied that the obtained compound could have composition different from that of the binary γ-Sn_3N_4 due to a possible contamination with oxygen and/or carbon. A detailed consideration of this issue is given in the Electronic Supplementary Material to the present paper.

In this work, we synthesised γ-Sn_3N_4 from the elements at high pressures and temperatures in a laser heated diamond anvil cell (LH-DAC). The applied here procedure of the sample preparation and synthesis we consider as the most reliable way to obtain high-pressure nitrides with a negligible oxygen and/or carbon contamination. We collected Raman spectra of the products after the synthesis and upon pressure decrease and provided quantitative information of the Raman band frequencies and their pressure dependences. Furthermore, we examined the recovered product using powder XRD and performed, for the first time, the structure refinement for γ-Sn_3N_4 synthesised from the elements. From the measured pressure dependences of the observed Raman-band frequencies, we derived an average mode Grüneisen parameter of γ-Sn_3N_4. The latter was used to estimate the thermal shock resistance of γ-Sn_3N_4 with respect to that of γ-Si_3N_4, another member of the spinel-nitrides family, and β-Si_3N_4 known to be highly thermal-shock resistant. This property could be of interest for the applications of γ-Sn_3N_4 in high-flux-density IR-LEDs operating in pulsed modes, e.g., in optical fibre communications. Such operation causes temporally- and locally non-uniform resistive heating and thermal expansion when high-density electric currents pass through the LED which can cause the material fracture.

Table 1. Frequencies of the Raman bands of γ-Sn_3N_4 at ambient conditions, ω_{i0}, initial slopes of their pressure dependences, $\partial\omega_i/\partial P$, and mode Grüneisen parameters, γ_i. The measured here ω_{i0} values are compared with those reported earlier [34].

ω_{i0} (cm^{-1})		$\partial\omega_i/\partial P$ (cm^{-1}/GPa) this work	γ_i this work
Ref. [34]	this work		
160			
252	231(3)	not determined	
420	419(1)	2.62(9)	0.99
~470 *	499(3)	~1.6	~0.50
529	531(3)	3.2(4)	0.95
626	628(1)	4.96(9)	1.25
~670 *	~680 (broad)	not determined	
	745(2)	5.5(1)	1.17

* our estimation

Table 2. Experimentally determined structural parameters for γ-Sn_3N_4 (space group $Fd3m$, No. 227, $Z = 8$, 2nd setting) obtained in this work and reported in the literature.

a_0 (Å)	x(N)	Reference
9.037(3)	0.25950(6)	[4]
9.0144(1)	n. a.	[34]
9.0187(5)	0.2575(14)	this work

Experiment

Here, γ-Sn_3N_4 was synthesised in a LH-DAC via the reaction of elemental tin with molecular nitrogen at pressures of 15.7 GPa and 20 GPa at high temperatures around 2000 °C. We used a DAC described in Ref. [37] which is well suited for heating of samples with intense IR-laser radiation (Nd-YAG- or CO_2-laser). The DAC was equipped with diamond anvils having unbevelled culets of ~400 μm in diameter. We used stainless-steel gaskets pre-indented to the thickness of ~60 μm. The sample was prepared in a way described earlier [38]: A plate of metallic tin of about 10 μm in thickness was loaded in a hole of ~150 μm in diameter drilled in the gasket and separated from the lower diamond anvil by a thin NaCl-layer. The latter prevented possible reaction of the metal with the diamond anvil or diffusion of carbon from the diamond anvil into the sample during the laser heating, as discussed in several publications e.g. [39, 40, 41, 42]. Apparently, the degree of contamination with carbon can be high if the heated sample is in contact with one of the diamond anvils, as was the case in Refs. [35, 36]. The Sn plate was embedded in the nitrogen pressure medium via compression of high-purity nitrogen gas (99.999%) in a gas-loader to 3000 atm. After the sealing of the gas between the diamond anvils, the Sn-plate was separated from the upper anvil by a nitrogen layer of 30-40 μm in thickness. Prior to the gas loading, the whole sample assemblage in the DAC was dried in vacuum at 110 °C during 24 hours in order to remove any oxygen and humidity from the sample volume. Pressures in the compressed sample volume were measured using the calibrated shift of the R1 fluorescence line of ruby [43].

The laser-heating set-up was analogous to that described earlier [44, 45]: We used radiation of a Nd-YAG- or a CO_2-laser providing the maximal CW powers of ~35 W and ~200 W, respectively. In each case, the sample

was heated with slightly defocused laser radiation to temperatures around 2000 °C. The latter was obtained from the fit of the Planck formula with a wavelength independent emissivity to the thermal emission spectrum collected from the centre of the laser-heated spot e.g.[45]. In order to ignite the reaction in the entire sample, the laser beam was scanned over its surface. Because the sample temperatures fluctuated during the chemical reaction and upon the laser-beam scanning, the reported here values are only approximates. The total duration of the laser heating was typically shorter than 5 minutes. After the temperature quenching, the reaction product was examined in-situ at high pressure and upon decompression using Raman spectroscopy. The spectra were excited with a blue solid-state laser (λ_L=473 nm) and collected with a high-resolution spectrometer equipped with a Peltier-cooled CCD detector.

The recovered samples were further examined using an XRD set-up consisting of a microfocus source delivering Mo $K\alpha$ radiation focused to a spot of less than 200 μm in diameter and an imaging plate detector. In order to obtain powder XRD patterns suitable for the structure refinement, the samples were rotated on a Gandolfi camera. This excluded (i) appearance of artificial diffraction peaks or peaks splitting when XRD-patterns are collected from a stationary polycrystalline sample containing a small number of crystallites of different size and (ii) graining of the scattered intensity when such a sample is rotated along a single axis. Two-dimensional XRD patterns recorded using the imaging plate detector were converted to standard one-dimensional patterns $I(2\theta)$ applying the Fit2D software [46]. In our previous studies on high-pressure nitrides of the group 4 elements, an identical XRD set-up was successfully used to determine structure of the cubic nitrides of Zr(IV) and Hf(IV), both having Th_3P_4-type structure, c-Zr_3N_4 and c-Hf_3N_4 [38].

Results and Discussion

Examination of the reaction products under an optical microscope revealed that the initially opaque metallic samples became transparent to visible light: If illuminated from below, the reaction products exhibited a brownish colour (**Figure 1**). This indicated the formation of a non-metallic tin nitride with a narrow band gap.

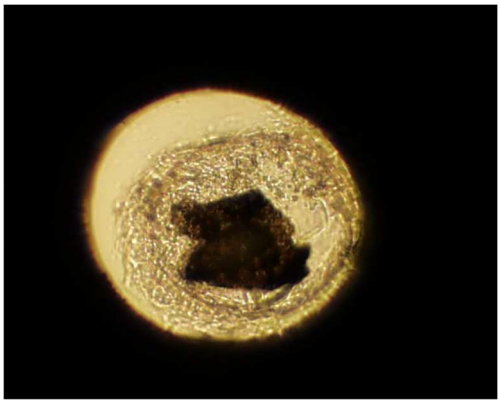

Figure 1. Optical image of the quenched product formed upon laser heating and reaction of tin with nitrogen at 20 GPa and ~2000 ºC. The sample in a DAC was illuminated from the bottom.

The product was also found to be Raman active. Its Raman spectra were measured at room temperature immediately after the temperature quenching and upon decrease of pressure to 1 atm. (10^{-4} GPa) (**Figure 2a**). In addition to the Raman peaks of γ-Sn_3N_4, we could detect two broad peaks of the nitrogen pressure medium, depending on the examined sample region. Their frequencies of ω=265 cm^{-1} and ω=375 cm^{-1} (measured at 20 GPa) agreed with those reported earlier [47]. Upon each pressure step, frequencies of all recognised Raman peaks of γ-Sn_3N_4 were recovered using the PeakFit program (Jandel scientific software): The spectra were divided in sections containing only one peak or two overlapping peaks. For each section, the background, approximated by a linear function, and the peaks, approximated by symmetric profile functions, were fitted simultaneously.

As seen in **Figure 2a**, intensities and shapes of some of the Raman peaks of γ-Sn_3N_4 changed with pressure: Two of the three broad Raman peaks, namely those at ω~540 cm^{-1} and ω~585 cm^{-1} (measured at P=20 GPa), narrowed on pressure decrease but the third one, at ω~780 cm^{-1} (measured at P=20 GPa), did not change its width significantly. Also, an additional low-frequency peak at ω=231(3) cm^{-1} was recognised at ambient conditions. Intensity of the highest-frequency Raman peak at ω=850 cm^{-1} (measured at 20 GPa) decreased upon

pressure release to a nearly undetectable level. Broadening and strong changes in intensities of the Raman peaks could be explained by a pronounced susceptibility to nonhydrostatic stress of samples in a DAC embedded in a solid pressure medium such as nitrogen or NaCl. However, a contribution of orientational dependences of the Raman peak intensities cannot be excluded for our samples because the number of crystallites irradiated with the focused laser beam was small and their positions changed upon pressure release due to a displacement of the DAC and/or of the sample with respect to the gasket.

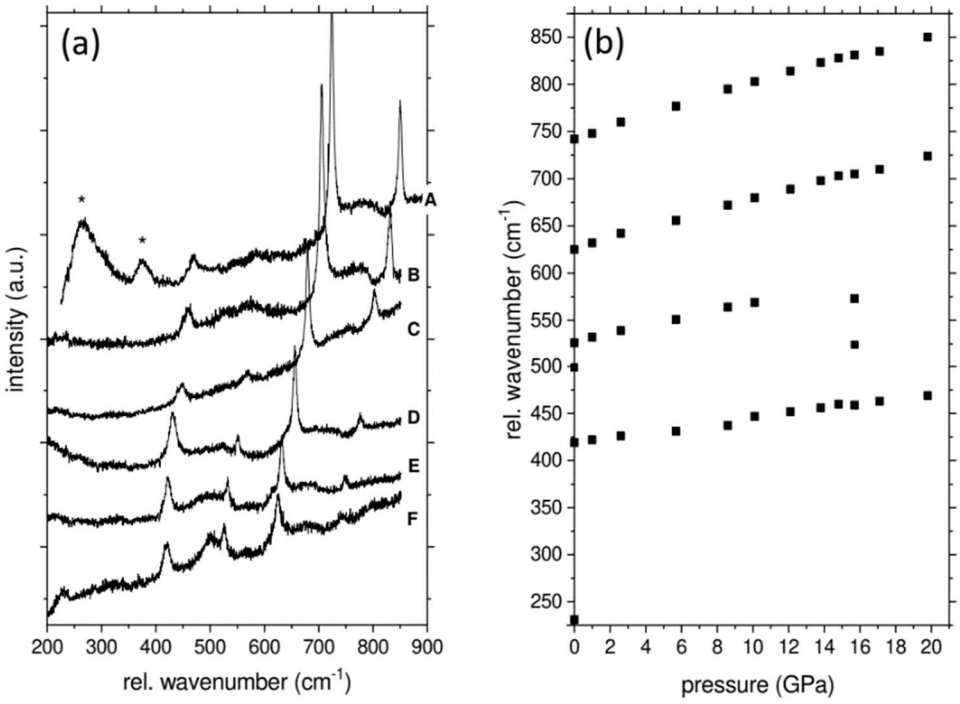

Figure 2. (a) Raman spectra of γ-Sn_3N_4 synthesized at high pressures via a reaction of tin with molecular nitrogen in a LH-DAC. A - Spectrum of the sample synthesised at 20 GPa showed, in addition to two broad peaks of the nitrogen pressure medium at ω=265 cm^{-1} and ω=375 cm^{-1} (stars), three strong and narrow Raman peaks as well as three weak and broad ones belonging to γ-Sn_3N_4. (B-F) Evolution of the Raman spectra of γ-Sn_3N_4 with pressure at RT. The spectra B, C, D, E, and F were measured at 15.7 GPa, 10.1 GPa, 5.7 GPa, 1.0 GPa, and 1 atm., respectively. (b) Pressure dependences of the Raman-band frequencies of γ-Sn_3N_4 shown in (a).

The Raman spectrum of the reaction product measured at 1 atm. (**Figure 2a, spectrum F**) was found to be similar to that of γ-Sn_3N_4 synthesised earlier by Shemkunas et al. [34] but some differences were also recognised: The three strongest peaks from our sample had frequencies of ω=419(1) cm^{-1}, ω=531(3) cm^{-1}, and ω=628(1) cm^{-1}, in agreement with the previous study (**Table 1**) but the peaks at ω=231(3) cm^{-1} and ω=499(3) cm^{-1} were significantly narrower than the earlier-detected features at ω~252 cm^{-1} and ω~470 cm^{-1} [34]. This broadening and shift of the Raman peaks in the previous work could be due to a partial substitution of nitrogen by oxygen and/or chlorine resulting in a distortion of the crystal lattice of γ-Sn_3N_4.

The measured spectra were used to derive pressure dependences of the Raman-band frequencies of γ-Sn_3N_4 (**Figure 2b**). Their values at ambient conditions, ω_{i0}, and the initial slopes, $\partial\omega_i/\partial P$, are summarised in **Table 1**. The earlier reported ω_{i0} values [34] are also shown for comparison.

Figure 3 shows a powder XRD pattern of our recovered product, obtained at P=20 GPa, after the background subtraction. Prior to the measurement, the sample was cleaned with distilled water to dissolve all NaCl grains still stuck to it and mounted on a Gandolfi camera. This approach permits collection of ideal powder XRD-patterns from polycrystalline samples containing only a limited number of grains. Analysis of the obtained diffractogram, $I(2\theta)$, revealed the presence of two compounds: γ-Sn_3N_4 and tetragonal β-Sn (a_0 = 5.831 Å and c_0 = 3.182, space group $I4_1/amd$, No. 141 [48]). Accordingly, we used the latter as an internal standard for scaling the refined cubic cell parameter a_0 of γ-Sn_3N_4 leading to its increase by 0.15%.

For our γ-Sn_3N_4, the Rietveld refinement yielded, after the scaling, a_0 = 9.0187(5) Å and x(N) = 0.2575(14). Here, we assumed that the cation and anion positions in the unit cell are fully occupied. The Bragg R-factor for

the γ-Sn_3N_4 phase was found to be R_{Bragg}=5.4. In **Table 2**, these values are compared with those obtained in the previous synthesis experiments [4, 34]. Our *x*-parameter agrees, within the experimental uncertainties, with that reported in the first publication on the structure solution and refinement of γ-Sn_3N_4 where large sample amounts were available for powder XRD measurements using a standard diffractometer [4].

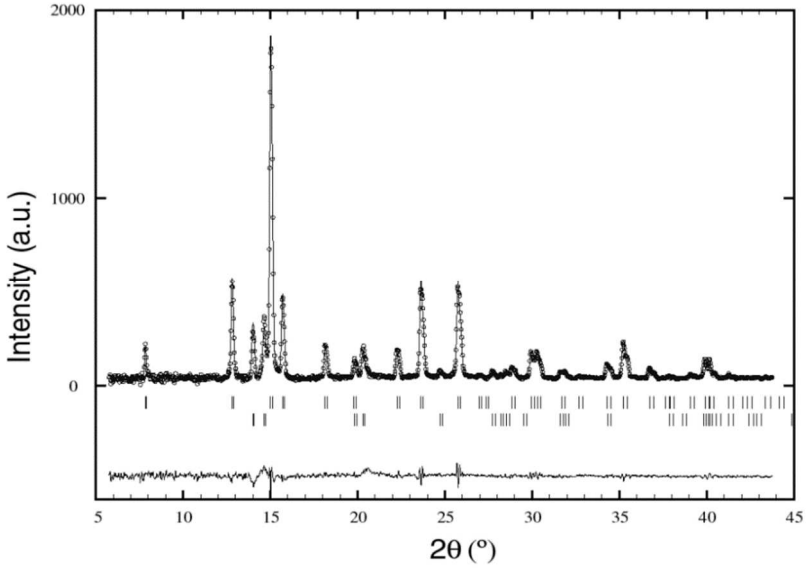

Figure 3. Result of the Rietveld-refinement of crystal structure of γ-Sn_3N_4 (solid line) based on the XRD powder pattern of the sample synthesised at 20 GPa and ~2000 ºC (circles). The pattern was obtained upon irradiation of the sample, rotated on a Gandolfi camera, with Mo$K\alpha$-radiation and the background was subtracted. A minor admixture of tetragonal β-Sn was present. Upper and bottom tick marks indicate positions of diffraction peaks of γ-Sn_3N_4 and β-Sn, respectively. The peak profiles were modelled by the pseudo-Voigt function. Our structure refinement resulted in R_{Bragg}=5.4 % and R_F = 5.6% for γ-Sn_3N_4 and in R_{Bragg} = 18.8 % and R_F = 11.1 % for β-Sn. The latter values we explain by a small amount of the β-Sn in the sample and by the overlapping of two of the four most intense diffraction peaks of β-Sn with the strong peaks of γ-Sn_3N_4. For the whole XRD-pattern, we obtained the global user-weighted χ^2=1.72. We note that Rietveld refinement of a XRD pattern with subtracted background always provide worse quality factors (e.g. R_{Bragg} and χ^2) when compared with the refinement of patterns containing background [83]. According to the author of the latter work, B. H. Toby, "the most important way to determine the quality of a Rietveld fit is by viewing the observed and calculated patterns graphically".

Applying the measured pressure dependences of the Raman band frequencies of γ-Sn_3N_4, $\partial\omega_i/\partial P$, and their values at ambient conditions, ω_{i0}, (**Figure 2b** and **Table 1**), we calculated mode Grüneisen parameters γ_i using the equation:

$$\gamma_i = \frac{B_0}{\omega_{i0}}\left(\frac{\partial \omega_i}{\partial P}\right)_T \quad (1)$$

where B_0 is bulk modulus of γ-Sn_3N_4 at ambient conditions. Here, we applied our recently measured value of B_0=158(11) GPa [49] (see also Electronic Supplementary Material) which confirms an earlier reported estimate of B_0 = 149(1) GPa [50]. The derived γ_i values (**Table 1**) were used to calculate the average mode Grüneisen parameter $\langle\gamma\rangle$ defined as

$$\langle\gamma\rangle = \Sigma C_i \cdot \gamma_i / \Sigma C_i \quad (2)$$

where C_i is the Einstein's heat capacity of the mode *i* [51-53]. For γ-Sn_3N_4, we obtained $\langle\gamma\rangle$=0.95 which is the first experimental information on Grüneisen parameter of this compound. This value is comparable with the thermodynamic Grüneisen parameter of γ-Si_3N_4, γ_{th} = 1.3, we calculated using the well-known equation:

$$\gamma_{th} = \frac{\alpha \cdot B_0}{C_V \cdot \rho} \quad (3)$$

where α is thermal expansion coefficient, ρ mass density, and C_V specific heat capacity per mass unit. For γ-Si_3N_4, we used the experimental values at atmospheric pressure: α=1.18·10^{-5} K^{-1} [54], B_0 =290 GPa [6],

$C_V \approx C_P = 91$ J/mol/K = 0.65 J/g/K [55], and $\rho = 4.022$ g/cm^3 [56]. A similar value of γ_{th}=1.194 was predicted for γ-Si_3N_4 from first principals [57] and the acoustic Grüneisen parameter of $\gamma_{el} \sim 1.2$ was estimated in model calculations [58].

Below we show that the knowledge of Grüneisen parameters allows a rough comparison of thermal shock resistances of solids if their hardnesses or yield stresses are known. According to the literature, thermal stress in a body of a regular shape, σ_t, subjected to a temperature difference ΔT, can be described by the equation

$$\sigma_t = A_1 \cdot \frac{E \cdot \alpha}{(1-\nu)} \Delta T \tag{4a}$$

or

$$\sigma_t = A_2 \cdot \frac{(1-\nu) \cdot E \cdot \alpha}{(1-2\nu)} \Delta T \tag{4b}$$

where A_1 and A_2 are numbers between 0 and 1 defined by the body shape, while E and ν are Young's modulus and Poisson's ratio, respectively [59, 60]. In general, the temperature difference, ΔT, between different positions in a body is defined by the difference in amount of heat delivered to the positions

$$\Delta Q = C_V \cdot \rho \cdot \delta v \cdot \Delta T \tag{5}$$

where δv is an (infinitesimally small) sample volume at each of the positions. Because Young's modulus can be expressed through bulk modulus and Poisson's ratio, $E = 3 \cdot B \cdot (1-2\nu)$ [61], **Equations 4** can be modified to

$$\sigma_t = 3A_1 \frac{(1-2\nu)}{(1-\nu)} \frac{\alpha \cdot B_0}{C_V \cdot \rho} \frac{\Delta Q}{\delta v} = 3A_1 \frac{(1-2\nu)}{(1-\nu)} \cdot \gamma_{th} \cdot \frac{\Delta Q}{\delta v} \sim Const_1 \cdot \gamma_{th} \cdot \Delta q \tag{6a}$$

or

$$\sigma_t = 3A_2(1-\nu) \frac{\alpha \cdot B_0}{C_V \cdot \rho} \frac{\Delta Q}{\delta v} = 3A_2(1-\nu) \cdot \gamma_{th} \cdot \frac{\Delta Q}{\delta v} \sim Const_2 \cdot \gamma_{th} \cdot \Delta q \tag{6b}$$

where $\Delta q = \Delta Q / \delta v$ is the difference in the heat densities delivered to the different body positions and *'Const'* represents a constant value. Here, we first used **Equation 3** describing thermal Grüneisen parameter and then substituted the expressions $3 \cdot A_1 \cdot (1-2\nu)/(1-\nu)$ and $3 \cdot A_2 \cdot (1-\nu)$ by $Const_1$ and $Const_2$, respectively, which only weakly depend on the body material. Obviously, such simplification is not necessary when elastic moduli of the materials of interest are well established. However, this is not the case for γ-Sn_3N_4. For hard ceramics, the approximation of the expressions $3 \cdot A_1 \cdot (1-2\nu)/(1-\nu)$ and $3 \cdot A_2 \cdot (1-\nu)$ by the constant values $Const_1$ and $Const_2$ holds reasonably well, especially if they belong to the same family: Our analysis of the data for several well-examined hard compounds (**Table 3**) showed that the ratio (1-2ν)/(1-ν) scatters with a low amplitude (for most of the compounds) around 0.76. The hexagonal β-Si_3N_4, and the conducting TiN and ZrN show lower values of 0.61-0.67 while diamond exhibits a high value of 0.93. Similarly, the value of $(1-\nu)$ varies, for most of the compounds, around 0.81 and, again, hexagonal β-Si_3N_4, and the conducting TiN and ZrN show lower values. Ceramics belonging to the same family show a much weaker scattering of $(1-2\nu)/(1-\nu)$ and $(1-\nu)$ (e.g. the monocarbides in **Table 3**). Moreover, this scattering is minor when compared with the differences in thermal shock resistances estimated below for γ-Sn_3N_4, γ-Si_3N_4 and β-Si_3N_4. Also, we do not further distinguish between $Const_1$ and $Const_2$ because the comparison is meaningful only for bodies having the same shape.

For any of the compounds, **Equations 6** permit determining of Δq_{max} describing the maximal contrast in the heat density above which the arising thermal stress exceeds tensile strength, $\sigma_t \geq \sigma_{TS}$, and thus causes irreversible damages. In case of ceramics, the main mechanism of the damages is fracturing quantified by the value of σ_{TS} which, in turn, is limited from above by the yield strength, σ_y [76]. Accordingly, for two bodies of the same shape made of ceramics having equal σ_y, a greater Grüneisen parameter implies failure at a lower Δq_{max}. For this reason, the ratio σ_y / γ_{th} can be used for a rough comparison of thermal shock resistances of ceramics. Because σ_y is proportional to hardness, $H_V \approx 3\sigma_y$, [76-78], the ratio H_V / γ_{th} can equally well be used for the comparison of thermal shock resistances of ceramics. The latter expression appears to be more useful because hardnesses rather than tensile- or yield strengths are reported in the literature.

Applying the measured here average mode Grüneisen parameter of γ-Sn_3N_4 of $\langle\gamma\rangle$=0.95 and the earlier reported Vickers microhardness of $H_V = 11$ GPa [10], we calculated the ratio $H_V / \langle\gamma\rangle = 12$ GPa. Here, $\langle\gamma\rangle$ of γ-Sn_3N_4 was used because its thermodynamic Grüneisen parameter is not known due to the unavailability of big samples needed to measure C_V or C_P. For comparison, we calculated H_V / γ_{th} for β-Si_3N_4, the well-known thermal-shock resistant ceramics, and for γ-Si_3N_4. Using the experimental value of $H_V = 20$ GPa for the densified polycrystalline β-Si_3N_4 sintered without any additives [79] and $\gamma_{th} = 0.59$, measured at room temperature [80], we obtained $H_V / \gamma_{th} = 34$ GPa. Similarly, applying the experimental $H_V = 35$ GPa measured for the densified

polycrystalline γ-Si_3N_4 [8] and the above calculated γ_{th} = 1.3, we obtained H_V/γ_{th} =27 GPa. Thus, γ-Sn_3N_4 is expected to exhibit a moderate thermal shock resistance when compared with the two phases of Si_3N_4 estimated to have comparable thermal shock resistances. On the other hand, it appears to exceed the thermal shock resistance of GaAs with a smaller ratio H_V/γ_{th} < 8 GPa which we calculated using the earlier reported hardness [81] and Grüneisen parameter [82].

Table 3. Experimental Poisson's ratios, ν, and the values of $(1-2\nu)/(1-\nu)$ and $(1-\nu)$ of several well-examined ceramic compounds. The main criteria for the data selection were: (i) The values are taken from the original publications; (ii) quality of the samples was stated; (iii) preference was given to the measurements on single crystals and ν was derived using the Hill approximation; (iv) experimental results for films were included only when reliable data for bulk samples were not available.

Compound	ν	$(1-2\nu)/(1-\nu)$	$(1-\nu)$	Reference
α-SiC	0.16	0.81	0.84	[62]
β-SiC	0.17	0.80	0.83	[63]
TiC	0.19	0.77	0.81	[64]
ZrC	0.20	0.76	0.80	[64]
VC	0.21	0.74	0.79	[65]
WC	0.23	0.69	0.77	[66]
β-Si_3N_4	0.28	0.61	0.72	[67]
γ-Si_3N_4	0.18	0.78	0.82	[8]
TiN	0.25	0.67	0.75	[68]
ZrN	0.25	0.67	0.75	[69]
TiB_2	0.10	0.88	0.90	[70]
ZrB_2	0.13	0.85	0.87	[71]
B_4C	0.17	0.79	0.83	[72]
B_6O	0.16	0.82	0.84	[73]
β-B	0.13	0.85	0.87	[73]
c-BN	0.12	0.87	0.88	[74]
Diamond	0.07	0.93	0.93	[75]

Conclusions

The reported here synthesis of γ-Sn_3N_4 from the elements demonstrated that this compound is thermodynamically stable at pressures between 16-20 GPa and temperatures around 2000 °C. The brownish colour of the sample indicated that γ-Sn_3N_4 is a narrow-band-gap semiconductor. This is in agreement with the earlier soft X-ray spectroscopic measurements reporting the band gap of E_g = 1.6(2) eV, predicted to be direct [17] and disproves the much smaller E_g =0.5 eV recently calculated in Ref. [36]. The measured pressure dependences of the Raman-active bands of γ-Sn_3N_4 were used to derive its average mode Grüneisen parameter $\langle\gamma\rangle$=0.95. The latter value permitted the estimation of thermal shock resistance of γ-Sn_3N_4 using the developed here approach. Comparison with two polymorphs of silicon nitride suggested that, among the three materials, β-Si_3N_4 exhibits the highest thermal shock resistance but that of γ-Si_3N_4 is similarly high. The thermal shock resistance of γ-Sn_3N_4 appears to be moderate but better than that of GaAs presently used for the fabrication of IR-LEDs.

Acknowledgments

This work has been carried out within the framework of the EUROfusion Consortium and has received funding from the Euratom research and training programme 2014-2018 and 2019-2020 under grant agreement No 633053. The views and opinions expressed herein do not necessarily reflect those of the European Commission. Technical support of R. Boehler is acknowledged.

References

1. Leinenweber, K., O'Keeffe, M., Somayazulu, M., Hubert, H., McMillan, P. F. & Wolf, G. H. 1999. Synthesis and structure refinement of the spinel, □-Ge_3N_4. *Chem. Eur. J.* **5**, 3076-3078. (doi 10.1002/(SICI)1521-3765(19991001)5:10%3C3076::AID-CHEM3076%3E3.0.CO;2-D)
2. Serghiou, G., Miehe, G., Tschauner, O., Zerr, A. & Boehler, R. 1999. Synthesis of a cubic Ge_3N_4 phase at high pressures and temperatures. *J. Chem. Phys.* **111**, 4659-4662. (doi 10.1063/1.479227)
3. Zerr, A., Miehe, G., Serghiou, G., Schwarz, M., Kroke, E., Riedel, R., Fueß, H., Kroll, P. & Boehler, R. 1999. Synthesis of cubic silicon nitride. *Nature* **400**, 340-342. (doi 10.1038/22493)
4. Scotti, N., Kockelmann, W., Senker, J., Traßel, S. & Jacobs, H. 1999. Sn_3N_4, a tin(IV) nitride - Syntheses and the first crystal structure determination of a binary tin-nitrogen compound. *Z. Anorg. Allg. Chem.* **625**, 1435-1439. (doi 10.1002/(SICI)1521-3749(199909)625:9%3C1435::AID-ZAAC1435%3E3.0.CO;2-%23)
5. Soignard, E., McMillan, P. F. & Leinenweber, K. 2004. Solid solutions and ternary compound formation among Ge_3N_4-Si_3N_4 nitride spinels synthesized at high pressure and high temperature. *Chem. Mater.* **16**, 5344-5349. (doi 10.1021/cm048930v)
6. Zerr, A., Kempf, M., Schwarz, M., Kroke, E., Göken, M. & Riedel, R. 2002. Elastic moduli and hardness of cubic silicon nitride. *J. Am. Ceram. Soc.* **85**, 86-90. (doi 10.1111/j.1151-2916.2002.tb00044.x)
7. Jiang, J. Z., Kragh, F., Frost, D. J., Stahl, K. & Lindelov, H. 2001. Hardness and thermal stability of cubic silicon nitride. *J. Phys. : Condens. Matter* **13**, L515-L520. (doi 10.1088/0953-8984/13/22/111)
8. Nishiyama, N., Ishikawa, R., Ohfuji, H., Marquardt, H., Kurnosov, A., Taniguchi, T., Kim, B. N., Yoshida, H., Masuno, A., Bednarcik, J., et al. 2017. Transparent polycrystalline cubic silicon nitride. *Sci. Rep.* **7**, 44755. (doi 10.1038/srep44755)
9. Nishiyama, N., Langer, J., Sakai, T., Kojima, Y., Holzheid, A., Gaida, N. A., Kulik, E., Hirao, N., Kawaguchi, S. I., Irifune, T., et al. 2019. Phase relations in silicon and germanium nitrides up to 98GPa and 2400 degrees C. *J. Am. Ceram. Soc.* **102**, 2195-2202. (doi 10.1111/jace.16063)
10. Shemkunas, M. P., Petuskey, W. T., Chizmeshya, A. V. G., Leinenweber, K. & Wolf, G. H. 2004. Hardness, elasticity, and fracture toughness of polycrystalline spinel germanium nitride and tin nitride. *J. Mater. Res.* **19**, 1392-1399. (doi 10.1557/JMR.2004.0186)
11. Zerr, A. 2008. Comments on "Hardness, elasticity, and fracture toughness of polycrystalline spinel germanium nitride and tin nitride," by MP Shemkunas, WT Petuskey, AVG Chizmeshya, K. Leinenweber, and GH Wolf J. Mater. Res. 19, 1392 (2004) : Reestablishing of elastic moduli for □-Ge_3N_4. *J. Mater. Res.* **23**, 3273-3274. (doi 10.1557/jmr.2008.0405)
12. Boyko, T. D., Bailey, E., Moewes, A. & McMillan, P. F. 2010. Class of tunable wide band gap semiconductors □-$(Ge_xSi_{1-x})_3N_4$. *Phys. Rev. B* **81**, 155207. (doi 10.1103/PhysRevB.81.155207)
13. Zerr, A., Riedel, R., Sekine, T., Lowther, J. E., Ching, W. Y. & Tanaka, I. 2006. Recent advances in new hard high-pressure nitrides. *Adv. Mater.* **18**, 2933-2948. (doi 10.1002/adma.200501872)
14. Mo, S.-D., Ouyang, L., Ching, W. Y., Tanaka, I., Koyama, Y. & Riedel, R. 1999. Interesting physical properties of the new spinel phase of Si_3N_4 and C_3N_4. *Phys. Rev. Lett.* **83**, 5046-5049. (doi 10.1103/PhysRevLett.83.5046)
15. Ching, W. Y., Mo, S.-D., Tanaka, I. & Yoshiya, M. 2001. Prediction of spinel structure and properties of single and double nitrides. *Phys. Rev. B* **63**, 064102. (doi 10.1103/PhysRevB.63.064102)
16. McMillan, P. F. 2002. New materials from high-pressure experiments. *Nature Mater.* **1**, 19-25.
17. Boyko, T. D., Hunt, A., Zerr, A. & Moewes, A. 2013. Electronic structure of spinel-type nitride compounds Si_3N_4, Ge_3N_4, and Sn_3N_4 with tuneable band gaps: Application to light emitting diodes. *Phys. Rev. Lett.* **111**, 097402. (doi 10.1103/PhysRevLett.111.097402)
18. Museur, L., Zerr, A. & Kanaev, A. 2016. Photoluminescence and electronic transitions in cubic silicon nitride. *Sci. Rep.* **6**, 18523. (doi 10.1038/srep18523)
19. Feldbach, E., Zerr, A., Museur, L., Kitaura, M., Manthilake, G., Tessier, F., Krasnenko, V. & Kanaev, A. 2021. Electronic band transitions in γ-Ge_3N_4. *Electron. Mater. Lett.* **17**, 315-323. (doi 10.1007/s13391-021-00291-y)
20. Chang, Y. L., Song, Y., Wang, Z. B., Helander, M. G., Qiu, J., Chai, L., Liu, Z. W., Scholes, G. D. & Lu, Z. H. 2013. Highly Efficient Warm White Organic Light-Emitting Diodes by Triplet Exciton Conversion. *Adv. Funct. Mater.* **23**, 705-712. (doi 10.1002/adfm.201201858)
21. Caskey, C. M., Seabold, J. A., Stevanovic, V., Ma, M., Smith, W. A., Ginley, D. S., Neale, N. R., Richards, R. M., Lany, S. & Zakutayev, A. 2015. Semiconducting properties of spinel tin nitride and other IV_3N_4 polymorphs. *J. Mater. Chemistry C* **3**, 1389-1396. (doi 10.1039/c4tc02528h)

22. Lima, R. S., Dionisio, P. H., Schreiner, W. H. & Achete, C. 1991. Magnetron Sputtered Tin Nitride. *Solid State Communications* **79**, 395-398. (doi 10.1016/0038-1098(91)90491-d)
23. Maruyama, T. & Morishita, T. 1995. Tin nitride thin films prepared by radio-frequency reactive sputtering. *J. Appl. Phys.* **77**, 6641-6645. (doi 10.1063/1.359075)
24. Sickafus, K. E., Grimes, R. W., Valdez, J. A., Cleave, A., Tang, M., Ishimaru, M., Corish, S. M., Stanek, C. R. & Uberuaga, B. P. 2007. Radiation-induced amorphization resistance and radiation tolerance in structurally related oxides. *Nat. Mater.* **6**, 217-223. (doi 10.1038/nmat1842)
25. Sickafus, K. E., Minervini, L., Grimes, R. W., Valdez, J. A., Ishimaru, M., Li, F., McClellan, K. J. & Hartmann, T. 2000. Radiation tolerance of complex oxides. *Science* **289**, 748-751. (doi 10.1126/science.289.5480.748)
26. Gilbert, C. A., Smith, R., Kenny, S. D., Murphy, S. T., Grimes, R. W. & Ball, J. A. 2009. A theoretical study of intrinsic point defects and defect clusters in magnesium aluminate spinel. *J. Phys.-Condes. Matter* **21**, 275406. (doi 10.1088/0953-8984/21/27/275406)
27. Schwarz, R. & Jeanmaire, A. 1932. Über die Ammonolyse von Zinn- und Bleitetrachlorid. *Ber. Dtsch. Chem. Ges.* **65**, 1443-1448. (doi 10.1002/cber.19320650842)
28. Janeff, W. 1955. Herstellung von Metallnitriden in der Glimmentladung und einige ihrer Eigenschaften. *Z. Phys.* **142**, 619-636. (doi 10.1007/BF01375138)
29. Maya, L. 1992. Preparation of tin nitride via an amide imide intermediate. *Inorg. Chem.* **31**, 1958–1960. (doi 10.1021/ic00036a044)
30. Maya, L. 1993. Deposition of crystalline binary nitride films of tin, copper, and nickel by reactive sputtering. *J. Vac. Sci. Technol. A* **11**, 604-608. (doi 10.1116/1.578778)
31. Maruyama, T. & Morishita, T. 1996. Copper nitride and tin nitride thin films for write-once optical recording media. *Appl. Phys. Lett.* **69**, 890-891. (doi 10.1063/1.117978)
32. Inoue, Y., Nomiya, M. & Takai, O. 1998. Physical properties of reactive sputtered tin-nitride thin films. *Vacuum* **51**, 673-676. (doi 10.1016/S0042-207X(98)00271-1)
33. Takahashi, N., Terada, K. & Nakamura, T. 2000. Atmospheric pressure chemical vapor deposition of tin nitride thin films using a halide source. *J. Mater. Chem.* **10**, 2835-2837. (doi 10.1039/B005032F)
34. Shemkunas, M. P., Wolf, G. H., Leinenweber, K. & Petuskey, W. T. 2002. Rapid synthesis of crystalline spinel tin nitride by a solid-state metathesis reaction. *J. Am. Ceram. Soc.* **85**, 101-104. (doi j.1151-2916.2002.tb00047.x)
35. Niwa, K., Ogasawara, H. & Hasegawa, M. 2017. Pyrite form of group-14 element pernitrides synthesized at high pressure and high temperature. *Dalton Trans.* **46**, 9750-9754. (doi 10.1039/c7dt01583f)
36. Niwa, K., Inagaki, T., Ohsuna, T., Liu, Z., Sasaki, T., Gaida, N. A. & Hasegawa, M. 2020. Crystal structures and electronic properties of Sn_3N_4 polymorphs synthesized via high-pressure nitridation of tin. *Crystengcomm* **22**, 3531-3538. (doi 10.1039/d0ce00210k)
37. Chopelas, A. & Boehler, R. 1984. MgO:V^{2+} pressure scale for diamond anvil cells. *Material Res. Soc. Symp. Proc.* **22**, 274-278.
38. Zerr, A., Miehe, G. & Riedel, R. 2003. Synthesis of cubic zirconium and hafnium nitride having Th_3P_4-structure. *Nat. Mater.* **2**, 185-189. (doi 10.1038/nmat836)
39 Prakapenka, V. B., Shen, G. Y. & Dubrovinsky, L. S. 2003. Carbon transport in diamond anvil cells. *High Temp.-High Press.* **35-6**, 237-249. (doi 10.1068/htjr098)
40. Dewaele, A., Mezouar, M., Guignot, N. & Loubeyre, P. 2010. High melting points of tantalum in a laser-heated diamond anvil cell. *Phys. Rev. Lett.* **104**, 255701. (doi 10.1103/PhysRevLett.104.255701)
41. Morard, G., Boccato, S., Rosa, A. D., Anzellini, S., Miozzi, F., Henry, L., Garbarino, G., Mezouar, M., Harmand, M., Guyot, F., et al. 2018. Solving controversies on the iron phase diagram under high pressure. *Geophys. Res. Lett.* **45**, 11074-11082. (doi 10.1029/2018gl079950)
42. Liermann, H. P., Konopkova, Z., Appel, K., Prescher, C., Schropp, A., Cerantola, V., Husband, R. J., McHardy, J. D., McMahon, M. I., McWilliams, R. S., et al. 2021. Novel experimental setup for megahertz X-ray diffraction in a diamond anvil cell at the High Energy Density (HED) instrument of the European X-ray Free-Electron Laser (EuXFEL). *J. Synchrot. Radiat.* **28**, 688-706. (doi 10.1107/s1600577521002551)
43. Mao, H. K., Xu, J. & Bell, P. M. 1986. Calibration of the ruby pressure gauge to 800 kbar under quasi-hydrostatic conditions. *J. Geophys. Res.* **91**, 4673-4676. (doi 10.1029/JB091iB05p04673)
44. Boehler, R. 2000. High-pressure experiments and the phase diagram of lower mantle and core materials. *Rev. Geophys.* **38**, 221-245.
45. Zerr, A., Serghiou, G. & Boehler, R. 2000. Phase transitions and materials synthesis using the CO_2-laser heating technique in a diamond cell. In *Handbook of ceramic hard materials* (ed. R. Riedel), pp. 41-65. Weinheim, Germany, Wiley-VCH. (doi 10.1002/9783527618217.ch2)

46. Hammersley, A. P., Svensson, S. O., Hanfland, M., Fitch, A. N. & Hausermann, D. 1996. Two-dimensional detector software: From real detector to idealised image or two-theta scan. *High Pressure Res.* **14**, 235-248. (doi 10.1080/08957959608201408)
47. Schneider, H., Häfner, W., Wokaun, A. & Olijnyk, H. 1992. Room temperature Raman scattering studies of external and internal modes of solid nitrogen at pressures 8<P<54 GPa. *J. Chem. Phys.* **96**, 8046-8053. (doi 10.1063/1.462356)
48. PDF-2. 1996. Powder Diffraction File-2 Database. (JCPDS Int. Centre for Diffraction Data, Newtown Square, PA 19073, USA.
49. Zerr, A. et al. unpublished, 2022.
50. Pradhan, G. K., Kumar, A., Deb, S. K., Waghmare, U. V. & Narayana, C. 2010. Elastic and structural instability of cubic Sn_3N_4 and C_3N_4 under pressure. *Phys. Rev. B* **82**, 144112. (doi 10.1103/PhysRevB.82.144112)
51. Chopelas, A. 1990. Thermal properties of forsterite at mantle pressures derived from vibrational spectroscopy. *Phys. Chem. Minerals* **17**, 142-148. (doi 10.1007/BF00199666)
52. Chopelas, A. 1991. Thermal properties of □-Mg_2SiO_4 at mantle pressure derived from vibrational spectroscopy: implication for the mantle at 400 km depth. *J. Geophys. Res.* **96**, 11817-11829. (doi 10.1029/91JB00898)
53. Chopelas, A., Boehler, R. & Ko, T. 1994. Thermodynamics and behavior of □-Mg_2SiO_4 at high pressure: implications for Mg_2SiO_4 phase equilibrium. *Phys. Chem. Minerals* **21**, 351-359. (doi 10.1007/BF00203293)
54. Hintzen, H. T., Hendrix, M. R. M. M., Wondergem, H., Fang, C. M., Sekine, T. & de With, G. 2003. Thermal expansion of cubic Si_3N_4 with the spinel structure. *J. Alloys Comp.* **351**, 40-42. (doi 10.1016/S0925-8388(02)01065-4)
55. Nishiyama, N., Kitani, S., Ohta, Y., Kulik, E., Netriova, Z., Holzheid, A., Lences, Z., Kawaji, H. & Wakai, F. 2020. Low temperature heat capacity measurements of □-Si_3N_4 and □-Si_3N_4: Determination of the equilibrium phase boundary between □-Si_3N_4 and □-Si_3N_4. *J. Eur. Ceram. Soc.* **40**, 6309-6315. (doi 10.1016/j.jeurceramsoc.2019.11.025)
56. Schwarz, M., Miehe, G., Zerr, A., Kroke, E., Poe, B., Fuess, H., Rubie, D. C. & Riedel, R. 2000. Spinel-Si_3N_4: Multi-anvil press synthesis and structural refinement. *Adv. Mater.* **12**, 883-887. (doi 10.1002/1521-4095(200006)12:12<883::AID-ADMA883>3.0.CO;2-C)
57. Fang, C. M., de Wijs, G. A., Hintzen, H. T. & de With, G. 2003. Phonon spectrum and thermal properties of cubic Si_3N_4 from first-principles calculations. *J. Appl. Phys.* **93**, 5175-5180. (doi 0.1063/1.1566473)
58. Morelli, D. T. & Heremans, J. P. 2002. Thermal conductivity of germanium, silicon, and carbon nitrides. *Appl. Phys. Lett.* **81**, 5126-5128. (doi 10.1063/1.1533840)
59. Buessem, W. R. 1955. Thermal shock testing. *J. Am. Ceram. Soc.* **38**, 15-17. (doi 10.1111/j.1151-2916.1955.tb14546.x)
60. Kingery, W. D. 1955. Factors affecting thermal stress resistance of ceramic materials. *J. Am. Ceram. Soc.* **38**, 3-15. (doi 10.1111/j.1151-2916.1955.tb14545.x)
61. Landau, L. D. & Lifshitz, E. M. 1959. *Theory of elasticity*. London, Pergamon Press.
62. Kamitani, K., Grimsditch, M., Nipko, J. C., Loong, C.-K., Okada, M. & Kimura, I. 1997. The elastic constants of silicon carbide: A Brillouin-scattering study of 4H and 6H SiC single crystals. *J. Appl. Phys.* **82**, 3152-3154. (doi 10.1063/1.366100)
63. Djemia, P., Roussigne, Y., Dirras, G. F. & Jackson, K. M. 2004. Elastic properties of □-SiC films by Brillouin light scattering. *J. Appl. Phys.* **95**, 2324-2330. (doi 10.1063/1.1642281)
64. Chang, R. & Graham, L. J. 1966. Low-temperature elastic properties of ZrC and TiC. *J. Appl. Phys.* **37**, 3778-3783. (doi 10.1063/1.1707923)
65. Zhang, X., Comins, J. D., Every, A. G. & Stoddart, P. R. 1998. Surface Brillouin scattering studies on vanadium carbide. *Int. J. Ref. Met. Hard Mater.* **1998**, 303-308. (doi 10.1016/S0263-4368(98)00046-8)
66. Lee, M. & Gilmore, R. S. 1982. Single crytsal elastic constants of tungsten monocarbide. *J. Mater. Sci.* **17**, 2657-2660. (doi 10.1007/BF00543901)
67. Vogelgesang, R., Grimsditch, M. & Wallace, J. S. 2000. The elastic constants of single crystal □-Si_3N_4. *Appl. Phys. Lett.* **76**, 982-984. (doi 10.1063/1.125913)
68. Kim, J. O., Achenbach, J. D., Mirkarimi, P. B., Shinn, M. & Barnett, S. A. 1992. Elastic constants of single-crystal transition-metal nitride films measured by line-focus acoustic microscopy. *J. Appl. Phys.* **72**, 1805-1811. (doi 10.1063/1.351651)
69. Christensen, A. N., Dietrich, O. W., Kress, W. & Teuchert, W. D. 1979. Phonon anomalies in transition-metal nitrides: ZrN. *Phys. Rev. B* **19**, 5699-5703. (doi 10.1103/PhysRevB.19.5699)

70. Spoor, P. S., Maynard, J. D., Pan, M. J., Green, D. J., Hellmann, J. R. & Tanaka, T. 1997. Elastic constants and crystal anisotropy of titanium diboride. *Appl. Phys. Lett.* **70**, 1959-1961. (doi 10.1063/1.118791)
71. Okamoto, N. L., Kusakari, M., Tanaka, K., Inui, H., Yamaguchi, M. & Otani, S. 2003. Temperature dependence of thermal expansion and elastic constants of single crystals of ZrB_2 and the suitability of ZrB_2 as a substrate for GaN film. *J. Appl. Phys.* **93**, 88-93. (doi 10.1063/1.1525404)
72. Schwetz, K. A. & Grellner, W. 1981. The influence of carbon on the microstructure and mechanical properties of sintered boron nitride. *J. Less-Common Met.* **82**, 37-47. (doi 10.1016/0022-5088(81)90195-8)
73. Petrak, D. R., Ruh, R. & Atkins, G. R. 1974. Machanical properties of hot-pressed boron suboxide and boron. *Am. Ceram. Soc. Bull.* **53**, 569-573.
74. Grimsditch, M., Zouboulis, E. S. & Polian, A. 1994. Elastic constants of boron nitride. *J. Appl. Phys.* **76**, 832-834. (doi 10.1063/1.357757)
75. McSkimin, H. J. & Bond, W. L. 1957. Elastic moduli of diamond. *Phys. Rev.* **105**, 116-121. (doi 10.1103/PhysRev.105.116)
76. Ashby, M. F. & Jones, D. R. H. 1994. *Engineering Materials 2. An Introduction to Microstructures, Processing and Design*. Oxford, Pergamon Press.
77. Salmang, H. & Scholze, H. 1983. *Keramik. Teil 2: Keramische Werkstoffe*, 6 ed. Berlin, Springer-Verlag.
78. Ashby, M. F. & Jones, D. R. H. 1996. *Engineering Materials 1. An Introduction to their Properties and Applications*, 2nd ed. Oxford, Butterworth-Heinemann.
79. Tsukuma, K., Shimada, M. & Koizumi, M. 1981. Thermal conductivity and microhardness of Si_3N_4 with and without additives. *Am. Ceram. Soc. Bull.* **60**, 910-912.
80. Bruls, R. J., Hintzen, H. T., de With, G., Metselaar, R. & van Miltenburg, J. C. 2001. The temperature dependence of the Grüneisen parmeters of $MgSiN_2$, AlN and □-Si_3N_4. *J. Phys. Chem. Solids* **62**, 783-792. (doi 10.1016/S0022-3697(00)00258-4)
81. Yonenaga, I. 2005. Hardness, yield strength, and dislocation velocity in elemental and compound semiconductors. *Mater. Trans.* **46**, 1979-1985. (doi 10.2320/matertrans.46.1979)
82. Soma, T. & Kudo, K. 1980. Thermal expansion and pressure effect on the lattice vibration of tetrahedrally covalent compounds. *J. Phys. Soc. Jpn.* **48**, 115-122. (doi 10.1143/JPSJ.48.115)
83. Toby, B. H. 2006. R factors in Rietveld analysis: How good is good enough? *Powder Diffraction* **21**, 67-70. (doi 10.1154/1.2179804)

Additional Information

Data Accessibility
Data and materials are available upon request from the authors

Authors' Contributions
AZ: Conceptualization, Data curation, Formal analysis, Funding acquisition, Investigation, Methodology, Resources, Validation, Visualization, Writing – original draft, Writing – review & editing
GM: Data curation, Formal analysis, Investigation, Methodology, Writing – original draft, Writing – review & editing

Competing Interests
We have no competing interests